Available online at www.sciencedirect.com
ScienceDirect
Catalysis Today 133–135 (2008) 69–79
CATALYSIS TODAY
www.elsevier.com/locate/cattod

Synthesis of mesoporous ZSM-5 by crystallisation of aged gels in the presence of cetyltrimethylammonium cations

Marli Lansoni Gonçalves [a], Ljubomir D. Dimitrov [a,1], Maura Hebling Jordão [b], Martin Wallau [a,2], Ernesto A. Urquieta-González [a,*]

[a] *Universidade Federal de São Carlos, Departamento de Engenharia Química, C. Postal 676, Km. 235, CEP 13565-905, São Carlos, SP, Brazil*
[b] *Laboratório Nacional de Luz Sincrotron, C. Postal 6192-CEP 13083-970, Campinas, SP, Brazil*

Available online 1 February 2008

Abstract

ZSM-5 synthesis gels were aged during 18–72 h at temperatures between 30 and 90 °C. After addition of the cationic surfactant cetyltrimethylammonium bromide these so called ''seeding gels'' were crystallised at 120 or 150 °C. From gels aged at 60 °C, ZSM-5 crystals possessing uniform mesopores with diameters around 2.5 nm were obtained. SEM micrographs of these samples revealed, independently of the ZSM-5 crystallinity, a morphology typically for mesoporous MCM-41. Furthermore, the formation of a hexagonal mesopore array analogous to MCM-41, was indicated by X-ray diffraction (XRD). However, the symmetry of the mesopore array decreased with the ZSM-5 crystallinity of the samples, indicating the dislocation of the surfactant micelles during the transformation of the primary formed MCM-41 particles into ZSM-5. Otherwise, the crystallinity of the obtained ZSM-5 was influenced by the crystallisation temperature, by the time used in the seed ageing and by the Si/Al ratio of the gel.

Keywords: Mesoporous ZSM-5; MCM-41; Micro–mesoporous materials; Mesostructuration; Zeolite seeds

1. Introduction

Due to the Al-MCM-41 amorphous character, which results in comparison with microporous zeolites [1] in lower acidity [2] and hydrothermal stability [3], the application of those mesoporous aluminosilicates [4] as acid catalysts for the processing of bulky compounds is limited [5,6]. To overcome these limitations much effort has been done to combine the mesoporosity of mesoporous aluminosilicates with the acidity and stability of the microporous zeolites [7]. One of these attempts is the synthesis of ordered mesoporous aluminosilicates from solutions of zeolite precursors or ''seeding gels'' [8–11] in the presence of surfactants as mesostructure directing agents.

This method was introduced in 2000 by Liu et al. [9], who described the synthesis of mesoporous aluminosilicates from aged gels known to promote the crystallisation of Y zeolite [9], ZSM-5 or β zeolite [10]. To these so called ''seeding gels'', which are believed to contain precursors of the desired zeolite structure, they added a mesostructure directing surfactant. Although the mesoporous materials obtained by Liu et al. [9,10] do not show X-ray reflections in the wide angle range ($>5°2\theta$), they showed higher thermal stability than conventional mesoporous materials [7]. On the other hand, Huang et al. [8] and more recently Frunz et al. [11] and Gonçalves et al. [12] reported the crystallisation of mesoporous ZSM-5 crystals from the respective seeding gel in the presence of a cationic surfactant.

In this paper we will describe the influence of the ageing time, ageing temperature and aluminium content of the seeding gels as well as the influence of the crystallisation temperature on the formation of mesoporous ZSM-5 crystals in the presence of the cationic surfactant cetyltrimethylammonium bromide.

* Corresponding author.
E-mail address: urquieta@power.ufscar.br (E.A. Urquieta-González).
[1] Present address: Bulgarian Academy of Sciences, Noemvri Street, 1040 Sofia, Bulgaria.
[2] Present address: Universidade Federal de Pelotas, Instituto de Química e Geociências, Campus Universitário do Capão do Leão s/n, CEP 96010-900, Pelotas, RS, Brazil.

0920-5861/$ – see front matter © 2008 Elsevier B.V. All rights reserved.
doi:10.1016/j.cattod.2007.12.108

2. Experimental

2.1. Synthesis

The mesoporous ZSM-5 crystals were prepared by a two-step procedure, similar to that described by Liu et al. [10] for the preparation of steam-stable MSU-S. The respective seeding gels with a molar composition of: 1 SiO_2: x Al_2O_3: 0.2 TPAOH: 38 H_2O ($x = (SiO_2/Al_2O_3)^{-1}$; see Table 1), were prepared by dissolving sodium aluminate (82 mol.% of the required aluminium) in a solution (1 mol/L) of tetrapropylammonium hydroxide (TPAOH). After its complete dissolution, pyrogenic silica (Aerosil 380, Degussa AG, Germany) was added and the final SiO_2/Al_2O_3 ratio (Table 1) adjusted by the addition of aluminium nitrate nonahydrate (18 mol.% of the required aluminium). Subsequently the gel was stirred for 15 min and transferred into an autoclave, where it was aged under the conditions given in Table 1. Solid cetyltrimethylammonium bromide (CTAB) was added (SiO_2/CTAB = 3.85) and the mixture vigorously stirred until its complete dissolution. The crystallisation of the seeding gels was carried out using the conditions given in Table 1. Finally the solid was separated by filtration, washed with distilled water and dried, firstly for 24 h at 60 °C and subsequently for 24 h at 110 °C. The occluded surfactant (CTA^+) and the organic template (TPA^+) were removed by calcination in air at 550 °C for 10 h.

2.2. Characterisation

The solids were characterised by X-ray diffraction (XRD) (Cu Kα) in the wide angle range between 4 and 40°2θ (WAXRD) on a Siemens D5000 diffractometer and in the small angle range between 0.5 and 10°2θ (SAXRD) on a Rigaku Multiflex diffractometer.

The nitrogen sorption isotherms were obtained using a Quantachrome Corporation (Nova-1200) instrument. Prior to the analysis, approximately 0.05 g of each sample was treated under vacuum for 2 h at 150 °C. The specific surface area (S_{BET}) was estimated by the BET equation [13], while the pore size distribution (PSD) and the mesopore analysis were determined from the desorption, as well as, from the adsorption branch of the nitrogen isotherms using the Barrett–Joyner–Halenda (BJH) method [14]. The micropore volume was estimated by the t-plot analysis using the adsorption branch of the isotherms [15].

The infrared spectra were recorded using the KBr pellets and a PerkinElmer (Spectrum 100) FTIR Spectrometer in the range between 4000 and 400 cm^{-1}. The scanning electron microscopy (SEM) micrographs were obtained on a Zeiss DSM960 microscope operating at 30 kV and the transmission electron microscopy (TEM) analyses were realised in the National Synchrotron Light Laboratory (LNLS), Campinas, Brazil.

Table 1
SiO_2/Al_2O_3 ratio and the ageing and crystallisation conditions of the "seeding gels"

Sample	SiO_2/Al_2O_3	Ageing		Crystallisation	
		Temperature (°C)	Time (h)	Temperature (°C)	Time (h)
A	56	60	24	120	48
B	56	60	24	150	48
B2	56	30	48	150	72
B3	56	90	18	120	72
C	28	60	24	150	48
D	19	60	24	150	48
D2	19	60	48	150	24
D3	19	60	72	150	24
E	19	60	24	120	48

3. Results

3.1. X-ray diffraction

The XRD patterns of the calcined samples A–E, which differ in aluminium content and applied crystallisation temperature (see Table 1) are shown in Fig. 1. The SAXRD pattern of sample A (Fig. 1a) reveals three broad peaks at 2.50, 4.25 and 4.81°2θ (the last two are partially overlapped), attributable to the 100, 110 and 200 reflections of the two-dimensional hexagonal structure analogous to MCM-41 [4] with the respective parameter a_0 given in Table 2. For samples D and E, the SAXRD patterns (Fig. 1a) also show three peaks (partially overlapped) at 2.12, 3.56 and 4.30°2θ (sample D) and at 2.26, 3.83 and 4.61°2θ (sample E), corresponding to the two-dimensional hexagonal structures whose parameters a_0 are given in Table 2. In the range below 5.0°2θ, the SAXRD patterns of samples B and C (Fig. 1a) show only one broad peak at 2.05 and 1.92°2θ, respectively. The attribution of those peaks to the reflection of the 100 planes of a distorted hexagonal structure allows the estimation of a_0 by $a_0 = 2d_{100}\cdot 3^{-}$ and the respective values are given in Table 2.

Besides the peaks attributed to the two-dimensional hexagonal structure, Fig. 1a demonstrates peaks in the range higher than 5°2θ, which corresponds to the structure of microporous ZSM-5 [16]. Even for sample A, two small peaks can be identified at 8.05 and 8.96°2θ, which are shown in detail in Fig. 1b. The formation of ZSM-5 with high crystallinity is confirmed for samples B–D by the respective WAXRD patterns given in Fig. 1c. On the other hand, for sample E no peak, besides those of the mesoporous MCM-41 structure, can be observed in its WAXRD patterns, thus demonstrating the absence of crystalline ZSM-5.

In order to study the influence of the temperature and time used in the seed ageing, gels with compositions corresponding to those of samples B and D were aged under different conditions (Table 1). The SAXRD and the WAXRD patterns of samples prepared from seeding gels aged at 30 (sample B2), 60 (sample B) and 90 °C (sample B3) are compared in Fig. 2a and b, respectively. As it can be seen from Fig. 2a, a cubic mesophase analogous to MCM-48 [4] is obtained when the seeding gel was aged at 30 (sample B2) or 90 °C (sample B3). Furthermore, the WAXRD patterns of these samples (Fig. 2b) reveal that they do not contain any crystalline ZSM-5.

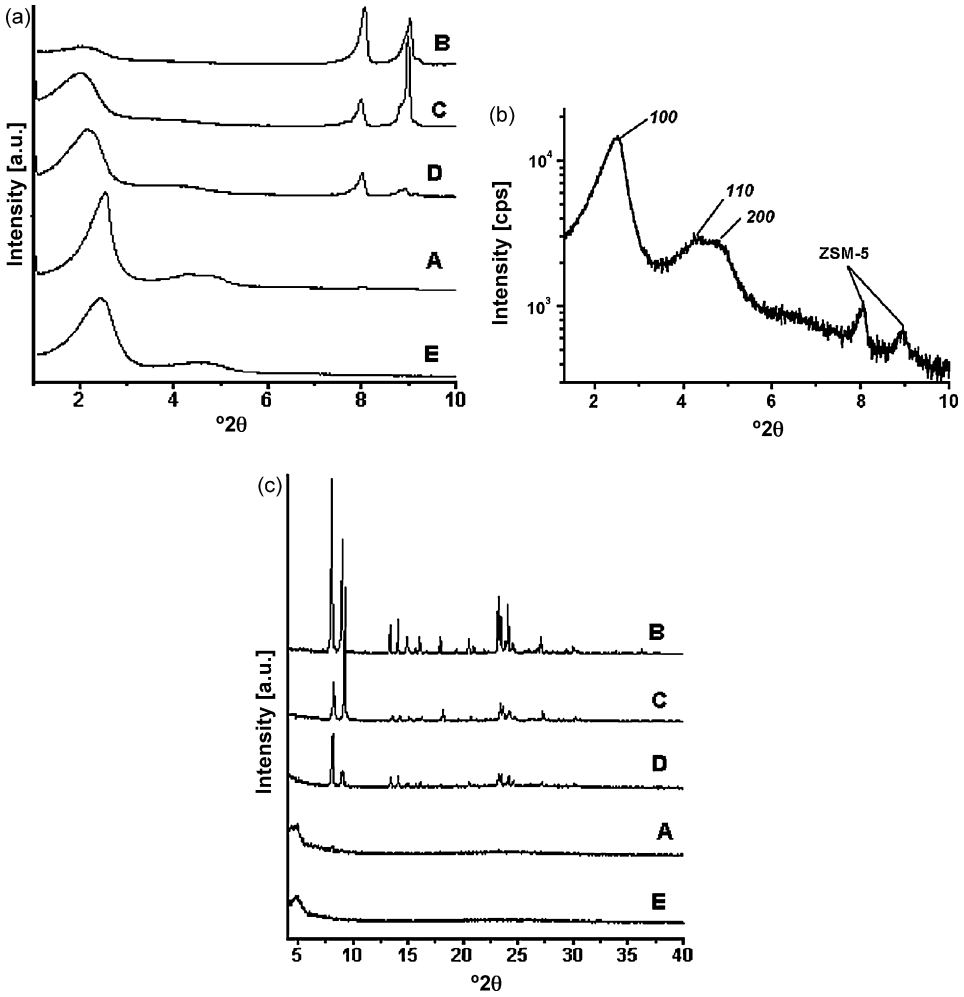

Fig. 1. (a) SAXRD patterns of calcined samples A–E; (b) detail of the pattern of sample A; (c) WAXRD patterns of calcined samples A–E.

Table 2
Textural and structural properties of the mesoporous structured solids

Sample	Mesoporous structure						Microporous ZSM-5		
	S_{BET} (m^2/g)	S_{ext} (m^2/g)	V_{tot} (cm^3/g)	d_p[a] (nm)	a_0[b] (nm)	t_w[c] (nm)	V_{mic} (cm^3/g)	t_{cryst}[d] (nm)	C_{XRD}[e] (%)
A	934	934	0.916	2.5	4.2	1.7[f]	0.000	53	n.d[g]
B	529	333	0.427	2.7	5.3	2.6[f]	0.088	86	98
B2	765	765	0.761	2.5	8.3	1.4[h]	–	–	–
B3	949	949	0.879	2.3	8.2	1.5[h]	–	–	–
C	597	521	0.524	2.7	4.9	2.2[f]	0.049	102	16
D	698	698	0.677	2.6	4.8	2.2[f]	0.000	52	12
D2	446	364	0.469	2.4	5.7	3.3[f]	0.045	66	62
D3	635	635	0.753	2.8	4.9	2.1[f]	0.000	46	32
E	826	826	0.841	2.5[i]	4.5	2.0[f]	–	–	–
ZSM-5[j]	–	–	–	–	–	–	–	75	100

[a] Mean pore diameter determined using the PSD obtained from the adsorption branch of the isotherms (Figs. 4 and 5).
[b] Unit cell parameter of the mesoporous structure determined by SAXRD.
[c] Wall thickness.
[d] Crystal thickness determined by the Scherrer formula [17].
[e] Relative XRD crystallinity.
[f] Determined as $t_w = a_0 - d_p$.
[g] Not determined (see text).
[h] Determined as $t_w = (a_0/3.092) - (d_p/2)$ [24].
[i] Determined using PSD obtained from the desorption branch (Fig. 4a).
[j] Commercial sample (SN-27, AlSi-Penta, Germany).

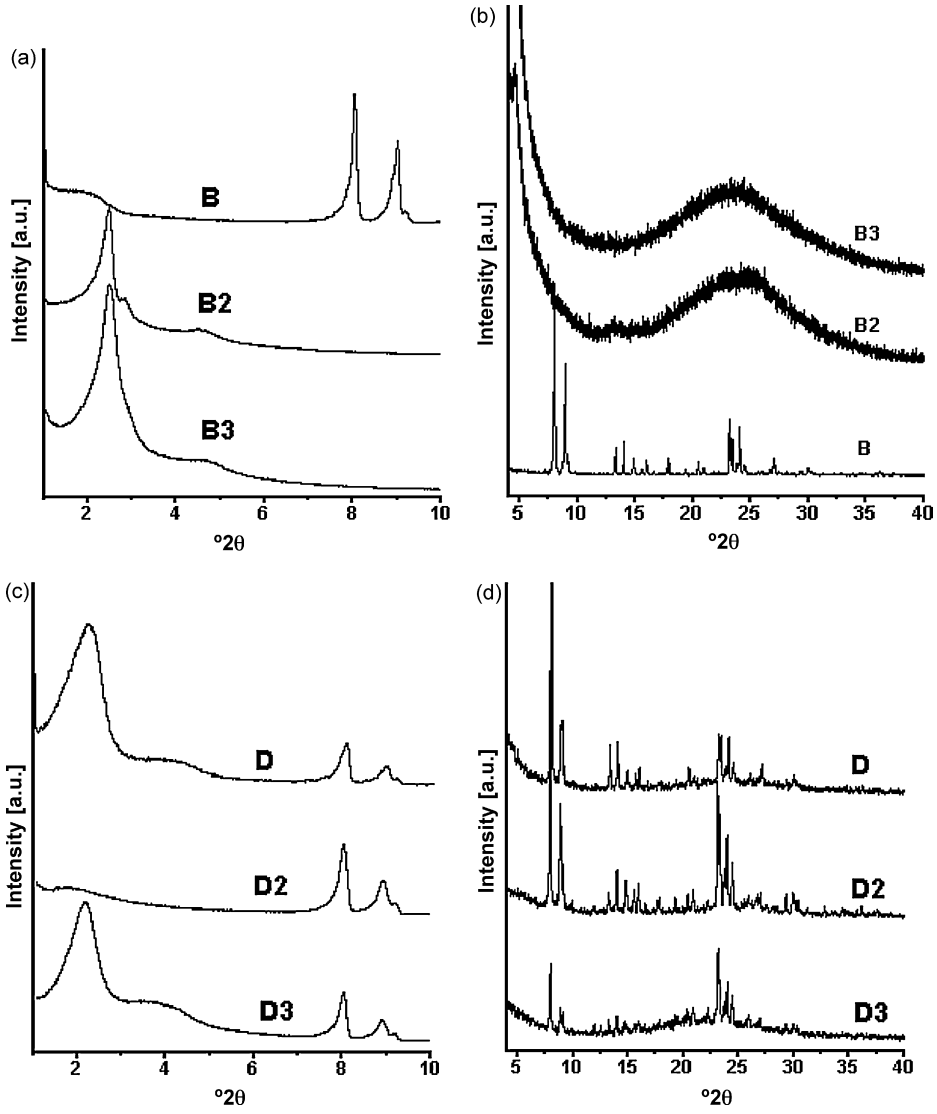

Fig. 2. (a) SAXRD patterns of calcined samples B, B2 and B3; (b) WAXRD patterns of calcined samples B, B2 and B3; (c) SAXRD patterns of calcined samples D, D2 and D3; (d) WAXRD patterns of calcined samples D, D2 and D3.

The influence of the duration of the seed ageing was studied in samples D, D2 and D3, where the seeding gel was aged for 24, 48 and 72 h, respectively. It can be seen from Fig. 2c and d that the increase of the duration from 24 to 48 increases the ZSM-5 crystallinity, however, a further increase of the ageing time to 72 h decreases the ZSM-5 crystallinity. Nevertheless, the crystallinity of sample D3 is still higher than that of sample D although the latter was crystallised for 48 h instead for 24 h.

The exact position, width and area of the peaks around 23.1 and 23.3°2θ, attributed to the 051 and −501 planes of the structure of calcined ZSM-5 [16], were determined from the WAXRD patterns given in Figs. 1c and 2d by fitting the peaks with a Gaussian function. These values allowed to estimate the thickness of the ZSM-5 crystallites (t_{cryst}) by the Scherrer formula [17] and, using a commercial ZSM-5 (SN-27, AlSiPenta GmbH, Germany) as reference, the relative XRD crystallinity (C_{XRD}). The obtained values are given in Table 2. Due to the low crystallinity of sample A, it was necessary to acquire its WAXRD pattern with a lower goniometer velocity (0.2°/min) than that used for the other samples (2°/min), so that here the peak area could not be used to determine its C_{XRD}.

3.2. Nitrogen sorption

The isotherms of the physisorption of nitrogen of the mesoporous samples A–E are shown in Fig. 3, and the specific surface area determined by the BET method [13] (S_{BET}), the external specific surface area (S_{ext}), the total specific pore volume (V_{tot}), and the specific micropore volume (V_{mic}) are demonstrated in Table 2. The isotherms in Fig. 3 can be classified following the IUPAC recommendations, as type IV, which are typical for mesoporous materials [18]. However, it can be observed that with the increase of the ZSM-5 crystallinity, the observed isotherms change from a typical type IV (samples A, E and D) to an intermediate between type IV and I (samples C and B), the latter indicative for the presence of micropores [18].

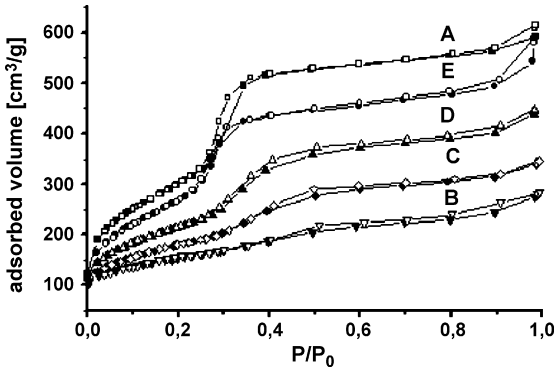

Fig. 3. Isotherms of nitrogen adsorption (closed symbols) and desorption (open symbols) of samples A–E.

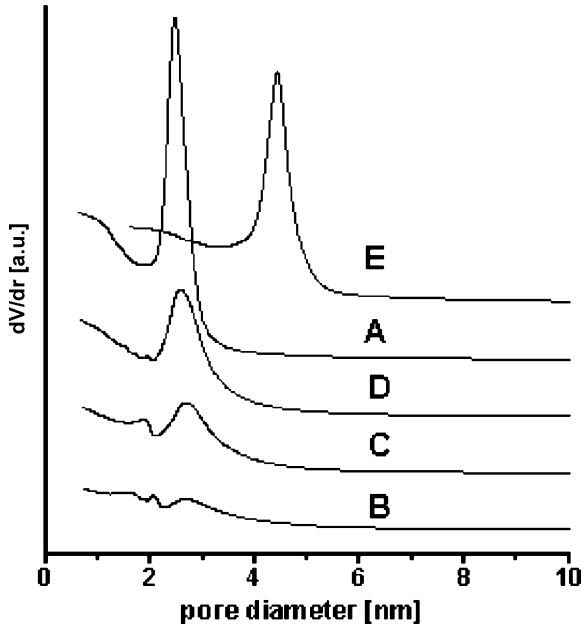

Fig. 4. Pore size distribution of samples A–E obtained by the BJH method [14] using the adsorption branch of the isotherms.

It can be seen from the data presented in Table 2 that S_{BET}, S_{ext} and V_{tot} decrease with increasing C_{XRD}, while V_{mic} increases. However, sample E, which does not contain crystalline ZSM-5 (Fig. 1c), possesses lower S_{BET}, S_{ext} and V_{tot} than sample A, which already contains small amounts of crystalline ZSM-5 (Fig. 1b). A possible explanation for the reduced mesoporosity of sample E might be associated with the higher aluminium content of the gel used for its synthesis. It was observed by different authors [19–21] that the incorporation of aluminium into MCM-41-like materials results in less ordered mesopore arrangements and increasing amounts of extra-framework aluminium. Both effects are reducing the specific surface area and the pore volume.

It should be further remarked that for samples A, D and D3 no microporosity was detected by the analysis of their nitrogen isotherms, although the presence of ZSM-5 was confirmed by their WAXRD patterns (Figs. 1b and c and 2d). This might be an indication for the formation of the ZSM-5 structure in the core of the MCM-41 particles. In this case, amorphous silica could be possibly precipitated on the formed ZSM-5 crystallites preventing the access of nitrogen molecules to their micropores. That amorphous silica is formed during the formation of mesoporous ZSM-5 was already observed by Frunz et al. [11].

The nitrogen isotherms of samples B2 and B3 (not shown) are also of type IV, as it is expected for mesoporous MCM-48. However, as it can be seen from the data given in Table 2, sample B2, which was prepared from a seeding gel aged at 30 °C, possesses significantly lower S_{BET}, S_{ext} and V_{tot} than sample B3, which was prepared from a seeding gel aged at 90 °C. This indicates that sample B2 contains unreacted amorphous silica. For samples D2 and D3 the nitrogen isotherms (not shown) demonstrated the presence of mesopores and allowed the detection of micropores for sample D2, the latter being attributed to the intrinsic microporosity of ZSM-5.

Fig. 4 shows the pore size distribution of samples A–E determined by the BJH method [14] from the adsorption branch of the nitrogen isotherms, which reveal for samples B–D mean pore diameters (d_p) near to 3 nm. On the other hand, when the PSD of these samples are obtained from the desorption branch (not shown) its width increases and d_p is shifted with increasing C_{XRD} to 4 nm. It was outlined by Groen et al. [22,23] that for pore diameters around 4 nm observed in the PSD obtained by the BJH method using the desorption branch of the nitrogen isotherms may be influenced by the so called tensile strength effect (TSE). TSE appears in the presence of interconnected pores with diameters higher than 4 nm, which have to empty through pores with diameters below 4 nm. This leads, in the case of nitrogen desorption at 77 K, to a forced closure of the hysteresis loop at relative pressures (P/P_0) around 0.42, which is interpreted in the PSD as uniform mesopores with diameters around 4 nm. Broadening of the PSD and shift of d_p towards 4 nm with increasing C_{XRD} are not observed in the PSD derived from the adsorption branch (Fig. 4). Therefore, for samples A–D the values of d_p given in Table 2 were determined from Fig. 4. On the other hand, a d_p of 4.4 nm as it is observed in Fig. 4 for sample E is physically implausible.

For an ideal hexagonal pore arrangement the wall thickness of the mesopores (t_w) is the difference between the unit cell parameter a_0 and d_p. Using the value of a_0 given in Table 2 and a mean pore diameter of 4.4 nm, t_w of sample E would be only 0.1 nm or less than the diameter of an O^{2-} ion (0.27 nm). Therefore, the pore diameter of 2.5 nm determined from the PSD obtained from the respective desorption branch of the isotherm (not shown), which results in t_w of 2.0 nm is more plausible. For samples B2 and B3, which possess MCM-48 structure, t_w was determined using a_0 and d_p by the method described by Schumacher et al. [24].

Besides the mesopores in the range between 2.3 and 2.8 nm, the PSD of samples B–D, D2 and D3 (see Figs. 4 and 5b) show the presence of an additional peak around 1.6–2.0 nm. It was outlined by Groen et al. [22,23] that this peak is an artefact caused by a phase transition (‘‘solidification’’) of the nitrogen adsorbed in the ZSM-5 micropores and therefore, it cannot be attributed to real pores.

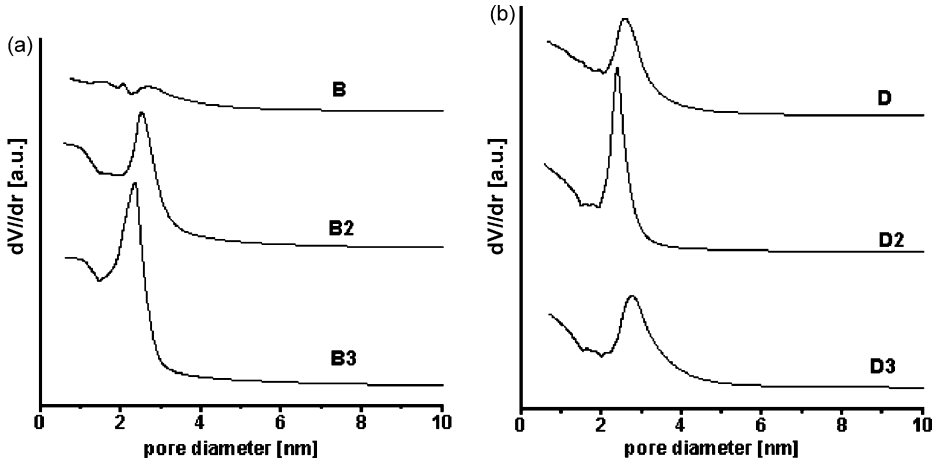

Fig. 5. Pore size distribution obtained by the BJH method [14] using the desorption branch of the isotherms: (a) samples B, B2 and B3; (b) samples D, D2 and D3.

3.3. IR spectroscopy (FTIR)

The FTIR spectra between 400 and 1300 cm^{-1} of the uncalcined samples A–E and the calcined samples A–D together with the spectrum of a commercial ZSM-5 (SN-27, AlSiPenta GmbH, Germany) are demonstrated in Fig. 6a and b, respectively. In this range all samples possess one broad band at 1000–1200 cm^{-1}, a shoulder at around 960 cm^{-1}, and three bands around 795, 546 and 450 cm^{-1}. Traditionally [25], the bands in the range at around 1000–1200 and 450 cm^{-1} are attributed to the structure insensitive internal tetrahedron asymmetric stretching vibrations and bending vibrations, respectively. The band at around 795 cm^{-1} can be attributed to both structure insensitive internal tetrahedron and structure sensitive external tetrahedron symmetric stretching vibrations [25]. The shoulder at around 960 cm^{-1} is attributed to terminal silanol groups on the wall surface of the mesopores [26]. The structure sensitive band [25], appearing in the presented spectra around 546 cm^{-1}, is attributed to five-ring units in the structures of pentasil zeolites like ZSM-5 [27].

The comparison of the FTIR spectra of the uncalcined samples A–D, given in Fig. 6a, reveals for the structure sensitive band at around 550 cm^{-1} that its width is curtailed while its intensity increased with increasing crystallinity of the ZSM-5. A similar observation was done by Kirschhock et al. [28], who observed for this band increase of its intensity and decrease of its width with increasing crystallinity together with a shift of its maximum from 600 to 550 cm^{-1}. While the increase of intensity was attributed by Kirschhock et al. [28] to an increase of the ZSM-5 crystallinity [27,29–31], they attributed the decrease in the width and frequency to an increase of the silicate entities containing five-rings together with an increase of their connectivity within the framework [28].

Frequently the ratio between the intensity of the structure sensitive band around 550 cm^{-1}, attributed to the five-rings of the pentasil structure and the intensity of the structure insensitive band around 450 cm^{-1}, attributed to internal tetrahedron vibrations [25], is taken as a measure for the crystallinity of the ZSM-5 zeolites [30,31]. It can be seen from Fig. 6a, that this 550/450 ratio is nearly the same for sample B and the commercial ZSM-5 zeolite, thus confirming their nearly identical C_{XRD} (Table 2). On the other hand, high 550/450 ratios are also observed for the uncalcined samples A and C. Furthermore, sample D shows a very broad adsorption in the

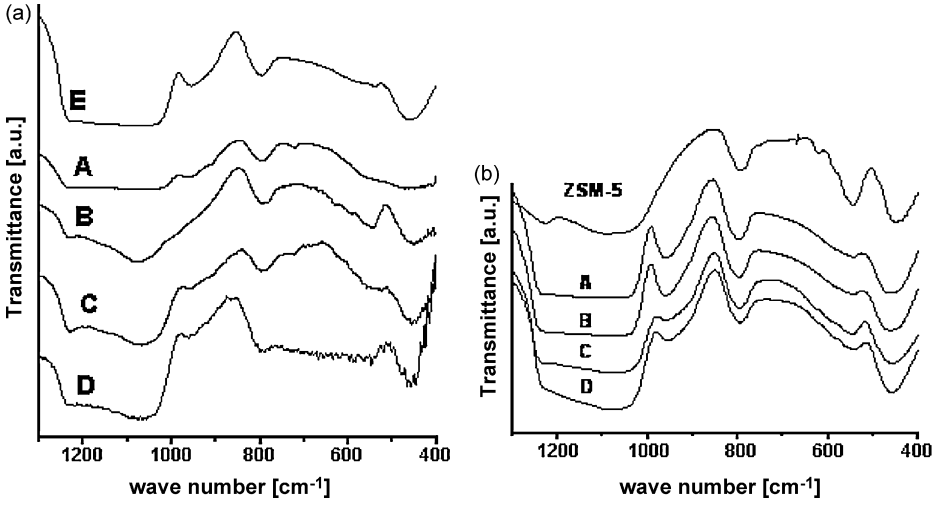

Fig. 6. FTIR spectra: (a) uncalcined samples A–E; (b) commercial ZSM-5 and calcined samples A–D.

range between 750 and 550 cm^{-1} (Fig. 6a), indicative for the presence of small rings in the silicate structure [28,32,33]. As samples A, C and D possess a much lower C_{XRD} than sample B and the commercial ZSM-5 (Table 2), the relative high adsorption at around 550 cm^{-1} (samples A and C) and at around 750–550 cm^{-1} (sample D) indicates the presence of a large number of X-ray amorphous ZSM-5 precursors and/or small silicate rings. Otherwise, a relatively low intensity of the structure sensitive band at around 550 cm^{-1} is observed for sample E, thus indicating that this sample contains only a small number of zeolite precursors. Here, it should be remarked that after calcination the intensities of the band at 550 cm^{-1}, for samples A and C, are markedly decreased. An intensity decrease is also observed in the spectrum of the calcined sample D (Fig. 6b). This decrease indicates that the zeolite precursors and silicate ring structures observed in the ''as made'' samples possess a low thermal stability.

A low intensity of the structure sensitive band at around 550 cm^{-1} is also observed in the spectra of the uncalcined samples B2 and B3 (Fig. 7a), thus demonstrating that only a small amount of ZSM-5 precursors was incorporated in the mesostructure when ZSM-5 seeding gels were aged at 30 °C (48 h) or 90 °C (18 h). On the other hand, the increase of the intensity of the band at around 550 cm^{-1} observed in the spectra of the calcined samples D, D2 and D3 (Fig. 7b), indicates that the prolongation of the seed ageing increases the number of ZSM-5 precursors incorporated in the mesoporous aluminosilicate.

3.4. Electron microscopy

3.4.1. Scanning electron microscopy

Fig. 8 shows the SEM micrographs of samples A–E, B2, B3, and D3. For samples A–E and D3, whose seeding gels were prepared at 60 °C, plate-like particles with a hexagonal crystal habit and lengths up to 200 nm are observed. Such particles with hexagonal habit are frequently observed for MCM-41 materials [34] and it should be emphasised that the particle morphology did not differ although these samples possess different relative ZSM-5 crystallinity, as it was demonstrated by XRD, FTIR and nitrogen sorption. Furthermore, it was not possible to observe isolated crystals, which would indicate the independent formation of microporous ZSM-5.

For samples B2 and B3 partly intergrown spherical particles with diameters up to 5 μm are observed. This morphology is similar to that observed by Bandyopadhyay and Gies [35] for MCM-48. Besides these smooth spherical MCM-48 particles, some intergrown lamellas (indicated by an arrow) and worm-like particles (indicated by a dotted arrow) are observed in sample B2, while some plate-like hexagonal similar to the MCM-41 particles in samples A–E and D3 (indicated by an arrow) are present in sample B3.

3.4.2. Transmission electron microscopy

Fig. 9 shows the TEM micrographs of samples B and C. These micrographs reveal that sample C still contains pores in hexagonal arrangement, while only disordered pores are observed in the TEM micrograph of sample B. Nevertheless, both samples show pores with uniform diameters around 2.5 nm, thus confirming the PSD determined from the nitrogen isotherms (Fig. 4). Furthermore, the micrographs in Fig. 9 suggest the same magnitude of the wall thickness (t_w) for samples B and C, comparing with the data obtained from nitrogen sorption and SAXRD (Table 2).

4. Discussion

As it was mentioned above (Section 3.4.1), the mesoporous ZSM-5 (samples A–D) and the mesoporous MCM-41 (sample E) possess, in spite of their different ZSM-5 crystallinity, the same morphology and no segregated particles, which would indicate the formation of ZSM-5 independently from the mesoporous structure. Therefore, the formation of the mesoporous ZSM-5 must proceed by an intraparticle transformation.

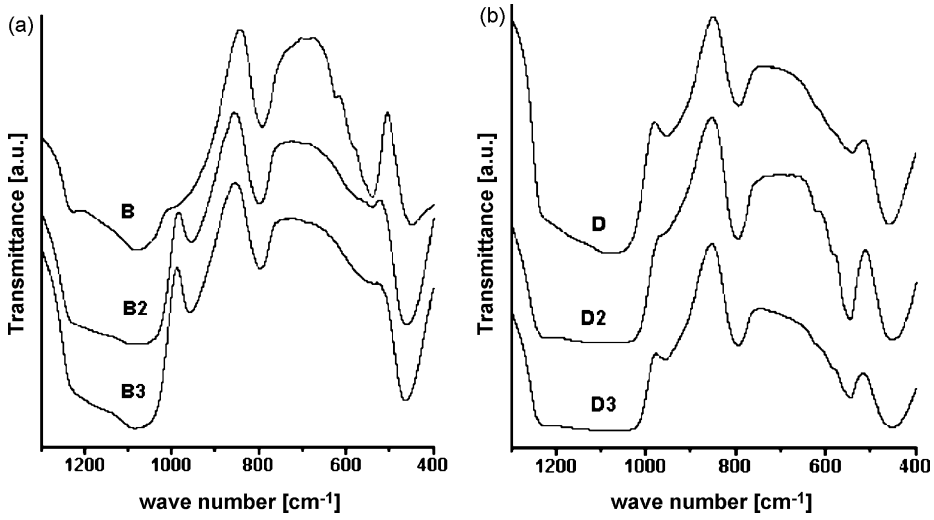

Fig. 7. FTIR spectra: (a) uncalcined samples B, B2 and B3; (b) calcined samples D, D2 and D3.

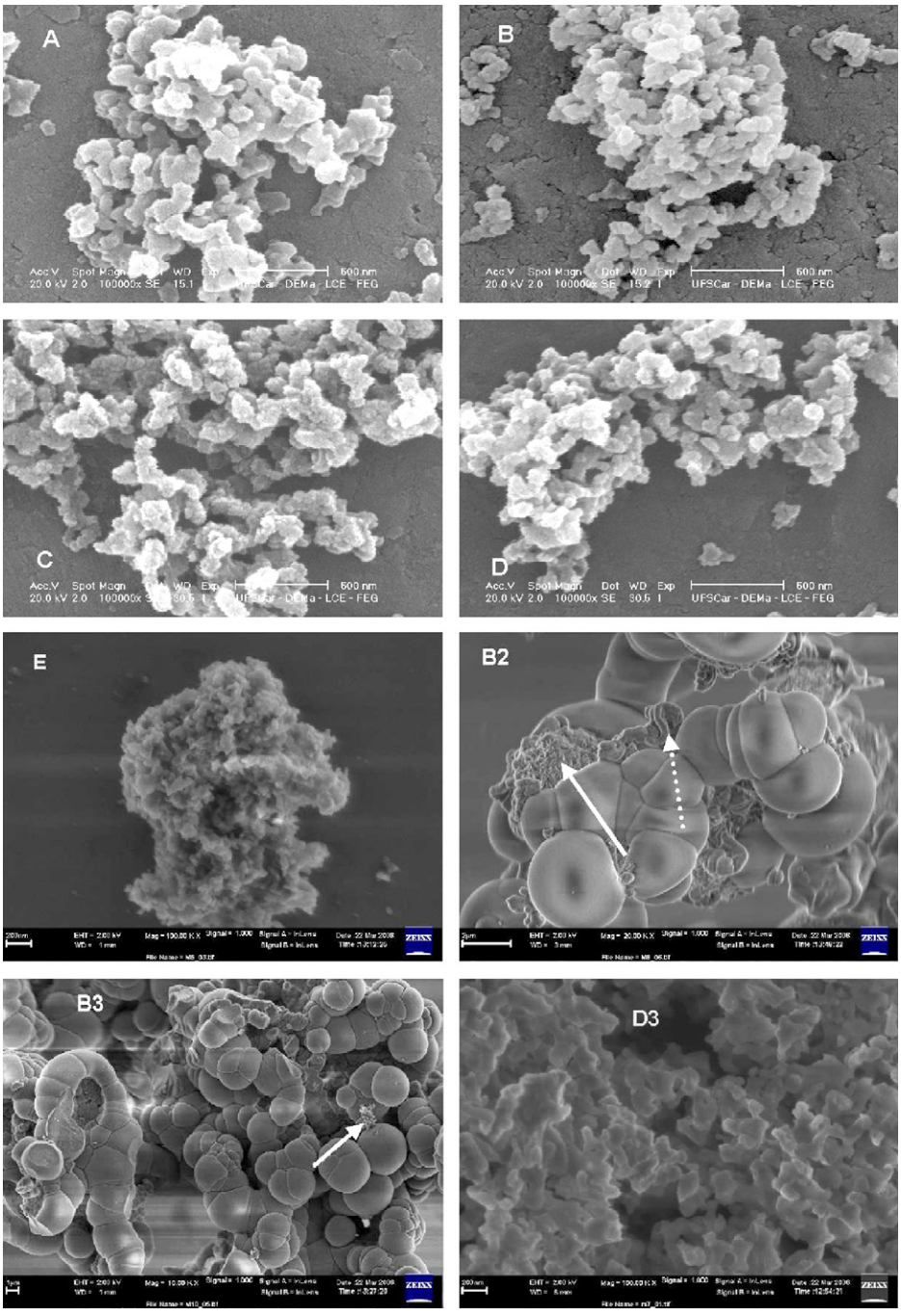

Fig. 8. SEM micrographs of samples A–E, B2, B3 and D3.

To understand such intraparticle transformation, one should remember that the prepared ''seeding gels'' are supposed to contain a large number of ZSM-5 precursors. Several hypothetical ZSM-5 precursors are described in the literature Kirschhock et al. [28,32], for example, identified in clear synthesis solutions of the pure siliceous counterpart of ZSM-5 (silicalite-1), colloidal particles with dimensions of 1.3 nm × 1.3 nm × 1.0 nm. It is further known that the mesoporous MCM-41 structure is, even at room temperature, formed within minutes after addition of the surfactant to the silica solution [36]. As the equivalent sphere diameter of 1.5 nm of the precursors described by Kirschhock et al [28,32] is smaller than t_w observed for the MCM-41 structure (Table 2), it might be possible that those precursors, or smaller units like double 3, 4 or 5 ring silicates become incorporated into the MCM-41 structure immediately after the addition of the surfactant. It is known that microporous zeolites can be formed by transformation of amorphous gels [37–41]. Therefore, the observed increase of the hexagonal unit cell and the wall thickness with increasing C_{XRD} (Table 2) indicates the transformation of the amorphous MCM-41 walls during the formation of the ZSM-5 structure. Such a transformation could explain the increase of the unit cell parameter and the wall thickness by decrease of the density from 2.25 g/cm^3

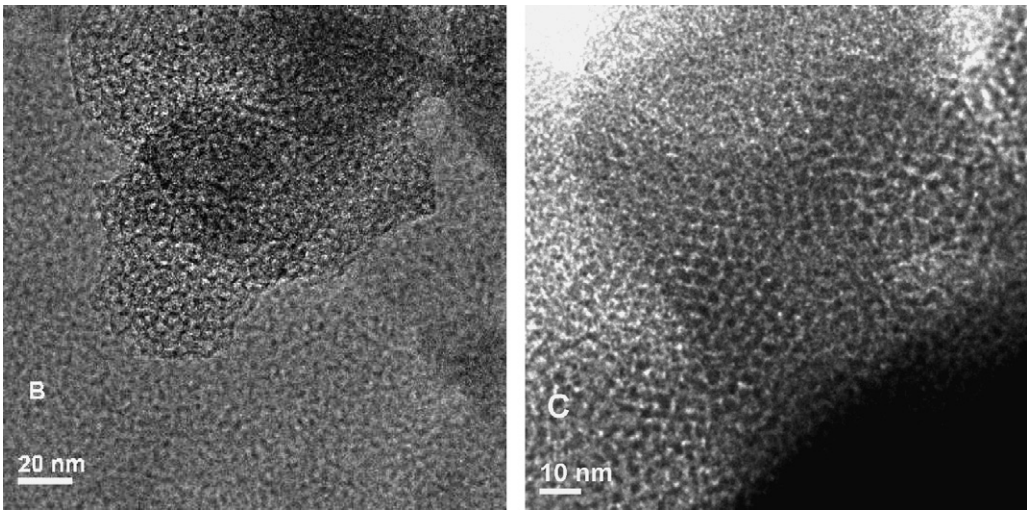

Fig. 9. TEM micrographs of samples B and C.

(amorphous silica [42]) to 1.79 g/cm^3 (ZSM-5 [1]). This density decrease expands the volume of the pore walls and therefore increases their thickness and the unit cell parameter. However, with proceeding crystallisation, the primary ZSM-5 precursors will form larger aggregates, like the particles with 2.8 and 10 nm in diameter described by de Moor et al. [43,44]. As such units are too large to be accommodated on the curvature of mesopores with diameters around 2.5 nm their formation leads to the observed collapse of the mesopore structure. Furthermore, the growing of the zeolite precursors, which consumes the MCM-41 walls, will form cavities with diameters larger than the original MCM-41 mesopores. The formation of such cavities with diameters larger than 4 nm during ZSM-5 crystallisation is indicated by the occurrence of TSE in the ZSM-5 containing samples, which is caused, as already discussed (Section 3.2), by pores with diameters larger than 4 nm (the formed cavities), which have to empty through pores with smaller diameters (the remaining MCM-41 pores).

Taking into account that the crystallisation conditions applied here are very similar to those of the formation of MCM-41 [4], it is likely that the interactions between the organic surfactant molecules are larger than those between the inorganic silicate units [45]. Therefore, the surfactant micelles remain unmodified during the dissolution of the silica walls and may act as exo- [46] or hard-templates [47] during the formation of the ZSM-5 crystals, which would explain the presence of uniform mesopores in the obtained ZSM-5 crystals. However, during the formation of the ZSM-5 crystals, the original micelle array is disarranged as it is indicated by the SAXRD patterns of samples B–D, D2 and D3 (Figs. 1a and 2c) and by the TEM micrograph of sample B (Fig. 9).

The above described intraparticle amorphous solid to crystalline solid transformation may also explain the observed influence of the duration and the gel ageing temperature on the obtained mesoporous solids. It is very surprising that under the here studied conditions, mesoporous ZSM-5 is only formed from seeding gels which were aged at 60 °C and that ageing at lower or higher temperatures impedes not only the formation of ZSM-5, but also leads to the formation of a different mesoporous structure. A possible explanation for this influence of the ageing temperature might be the different solubility and polymerisation degree of the silica at different temperatures. In general, the polymerisation degree of the silica decreases with increasing temperature and increases with increasing amount of dissolved silica [48]. It was already mentioned (see Section 3.2) that sample B2, prepared from a gel aged at 30 °C might still contain unreacted amorphous silica. Therefore, the liquid phase of the gel aged at 30 °C will contain a higher amount of less polymerised silica than that aged at 60 °C. The presence of less polymerised silica, which possesses a higher charge density, favours the formation of the cubic MCM-48 structure [49,45], thus explaining its formation from the seeding gel aged at 30 °C. As the degree of polymerisation also decreases with increasing temperature [49], the silica in the gel aged at 90 °C will also contain less polymerised silica than that aged at 60 °C and therefore favouring the formation of MCM-48. The fact that MCM-48 is not transformed into ZSM-5 is probably due to the low number of precursors embedded in the pore walls indicated by the FTIR spectra of the uncalcined samples B2 and B3 (Fig. 7a). The reason why the number of ZSM-5 precursors in the walls of samples B2 and B3 is too low to initiate the crystallisation might be their small wall thickness of 1.4 and 1.5 nm, which does not allow the incorporation of ZSM-5 precursors.

Otherwise, we observed that under similar conditions, an increase of the duration of the aging of the seeding gel from 24 h (sample D) to 48 or 72 h (samples D2 and D3) results in a much faster transformation of the mesoporous aluminosilicate into ZSM-5, indicating that a longer duration of the gel ageing increases the number of formed ZSM-5 precursors. The results of Huang et al. [8] and Frunz et al. [11], who aged their gels at the same temperature (25 °C) but for different times, also showed that an increased of the duration of the gel ageing increases the number of ZSM-5 precursors. The former authors aged the gels only for 1–4 h and observed after crystallisation for 6 days micron-sized ZSM-5 crystals. The latter authors, who aged the seeding gels for 24–48 h, obtained much smaller crystals of around 100 nm within 48 h, thus confirming that the

increase of the seed ageing period increases the number of ZSM-5 nuclei.

However, there is no simple relation between the gel ageing time and the formation of crystalline ZSM-5 during the crystallisation of the seeding gels in the presence of CTA^+, as it can be seen comparing samples D, D2 and D3. Although sample D3 prepared from a gel aged for 72 h possesses higher crystallinity than sample D, aged for 24 h, its C_{XRD} was lower than that of sample D2 prepared from a gel aged for 48 h. A possible explanation for this behaviour is that during the gel ageing of sample D3 not only the formation of the primary ZSM-5 precursors increases with increasing duration of the gel ageing but also increases their aggregation into larger particles, which cannot be incorporated into the MCM-41 pore walls. Therefore, the gel of sample D3 would, due to an increased in the duration of the gel ageing, contain more ZSM-5 precursors than the gel of sample D2, but due to the aggregation of part of these precursors into larger particles not all of them would be incorporated into the pore walls, thus explaining the slower formation of ZSM-5.

5. Conclusion

The discussed results show that solids with high crystalline ZSM-5, elevated external surface area, high pore volume and regular mesopores are obtained from an aged ZSM-5 synthesis gel which is crystallised in the presence of the cationic surfactant CTAB. Despite the fact that the final gel composition and the crystallisation conditions used by Liu et al. [10] were nearly identical to our synthesis conditions, these authors did not observe the formation of crystalline ZSM-5. As the IR spectra presented in their work, indicated the presence of a low amount of ZSM-5 precursors in the final mesoporous silicates, the absence of crystalline ZSM-5 might be attributed to either a less active silica source or to a lower ageing temperature, or yet, to a shorter ageing time. The fact that the results of Liu et al. [10] differs from that described here although the synthesis conditions used by them are very similar to those used here indicates that the parameters of the seeding gel preparation can be varied only in a small range. In the present study, we found that mesoporous ZSM-5 crystals were obtained only from seeding gels aged at 60 °C and that, under these conditions, the transformation of the primary formed MCM-41 into ZSM-5 increases with the increase of the ageing time from 24 to 48 h. However, a further prolongation of the ageing time decreases the formation of ZSM-5. As the ratio between the mesoporous structure and the ZSM-5 can be tailored by the duration of the seed aging and by the time and temperature of the crystallisation in the presence of CTA^+, the described synthesis method may allow the preparation of tailor-made catalysts for the transformation of bulky molecules.

Acknowledgements

The authors gratefully acknowledge the financial support provided by CNPq, Brazil (grant 477.759/2003-3 and 505157/2004-7) and the LME-LNLS for the TEM analyses. L.D.D. and M.W. also acknowledge PVE-Program/Capes, Brazil. Additional acknowledgement is given to Dr. A. Tißler (formerly AlSiPenta GmbH, now Südchemie AG) for providing the reference ZSM-5 sample (SN-27).

References

[1] W.M. Meier, D.H. Olson, Ch. Baerlocher, Zeolites 17 (1996) 1.
[2] M. Wallau, R.A.A. Melo, E.A. Urquieta-González, Stud. Surf. Sci. Catal. 146 (2003) 745.
[3] M. Wallau, R.A.A. Melo, E.A. Urquieta-González, Stud. Surf. Sci. Catal. 146 (2003) 303.
[4] J.S. Beck, J.C. Vartuli, W.J. Roth, M.E. Leonowicz, C.T. Kresge, K.D. Schmitt, C.T.-W. Chu, D.H. Olson, E.W. Shepard, S.B. McCullen, J.B. Higgins, J.L. Schlenker, J. Am. Chem. Soc. 114 (1992) 10834.
[5] D.T. On, D. Desplantier-Giscard, C. Danumah, S. Kaliaguine, Appl. Catal. A Gen. 253 (2003) 545.
[6] A. Taguchi, F. Schüth, Microporous Mesoporous Mater. 77 (2005) 1.
[7] J. Pérez-Pariente, I. Díaz, J. Agúndez, C.R. Chim. 8 (2005) 569.
[8] L. Huang, W. Guo, P. Deng, Z. Xue, Q. Li, J. Phys. Chem. B 104 (2000) 2817.
[9] Y. Liu, W. Zang, T.J. Pinnavaia, J. Am. Chem. Soc. 122 (2000) 8791.
[10] Y. Liu, W. Zhang, T.J. Pinnavaia, Angew. Chem. 113 (2001) 1295.
[11] L. Frunz, R. Prins, G.D. Pirngruber, Microporous Mesoporous Mater. 88 (2006) 152.
[12] M. L. Gonçalves, L.D. Dimitrov, M. Wallau, E.A. Urquieta-González, in: Proceedings of the 13 (Congresso Brasileiro de Catálise, 3), vol.3. Mercocat from September 11th to15th, 2005, Foz do Iguaçu, PR, Brazil, p. 1763.
[13] S. Brunauer, P.H. Emmet, E. Teller, J. Am. Chem. Soc. 60 (1938) 1553.
[14] E.P. Barret, L.G. Joyner, P.P. Halenda, J. Am. Chem. Soc. 73 (1951) 373.
[15] B.C. Lippens, B.G. Linsen, J.H. de Boer, J. Catal. 3 (1964) 32.
[16] M.M.J. Treacy, J.R. Higgins, H.v. Ballmoss, Zeolites 16 (1996) 524.
[17] B.D. Cullity, Elements of X-ray Diffraction, Addison-Wesley, Reading, 1967, p. 99.
[18] K.S.W. Sing, Pure Appl. Chem. 54 (1982) 2201.
[19] S. Gontier, A. Tuel, Stud. Surf. Sci. Catal. 105 (1997) 29.
[20] M. Janicke, D. Kumar, G.D. Stucky, B.F. Chmelka, Stud. Surf. Sci. Catal. 84 (1994) 243.
[21] M.T. Janicke, C.C. Landry, S.S. Christiansen, D. Kumar, G.D. Stucky, B.F. Chmelka, J. Am. Chem. Soc. 120 (1998) 6940.
[22] J.C. Groen, J. Pérez-Ramírez, Appl. Catal. A 268 (2004) 121.
[23] J.C. Groen, L.A.A. Peffer, J. Pérez-Ramíırez, Microporous Mesoporous Mater. 60 (2003) 1.
[24] K. Schumacher, P.I. Ravikovitch, A. Du Chesne, A.V. Neimark, K.K. Unger, Langmuir 16 (2000) 4648.
[25] E.M. Flanigen, H. Khatami, A. Seymenski, in: E.M. Flanigen, L.B. Sand (Eds.), Advance Chemistry Series 101, American Chemical Society, Washington, D.C, 1971, pp. 201–228.
[26] M.A. Camblor, A. Corma, J. Pérez-Pariente, J. Chem. Soc. Chem. Commun. (1993) 557.
[27] J.C. Jansen, F.J. van der Gaag, H. van Bekkum, Zeolites 4 (1984) 399.
[28] C.E.A. Kirschhock, R. Ravishankar, F. Verspeurt, P.J. Grobet, P.A. Jacobs, J.A. Martens, J. Phys. Chem. B 103 (1999) 4965.
[29] K.F.M.G.J. Scholle, W.S. Veeman, P. Frenken, G.P.M. van der Velden, Appl. Catal. 17 (1985) 233.
[30] R.M. Mohamed, O.A. Fouad, A.A. Ismail, I.A. Ibrahim, Mater. Lett. 59 (2005) 3441.
[31] S.R. Stojkovic, B.K. Adnadjevic, J. Serb. Chem. Soc. 54 (1989) 559.
[32] C.E.A. Kirschhock, R. Ravishankar, L. Van Looveren, P.A. Jacobs, J.A. Martens, J. Phys. Chem. B 103 (1999) 4972.
[33] R. Ravishankar, C. Kirschhock, B.J. Schoeman, P. Vanoppen, P.J. Grobet, S. Storck, W.F. Maier, J.A. Martens, F.C. De Schryver, P.A. Jacobs, J. Phys. Chem. B 102 (1998) 2633.
[34] S. Liu, L. Kong, X. Yan, A. He, Stud. Surf. Sci. Catal. 156 (2005) 379.
[35] M. Bandyopadhyay, H. Gies, C.R. Chim. 8 (2005) 621.
[36] M. Lindén, S.A. Schunk, F. Schüth, Angew. Chem. 110 (1998) 871.

[37] S. Mintova, N.H. Olson, V. Vatchew, T. Bein, Science 283 (1999) 958.
[38] M. Tsapatsis, M. Lovallo, M.E. Davis, Microporous Mater. 5 (1996) 381.
[39] W.H. Dokter, H.F. van Garderen, T.M.P. Beeleen, R.A. van Santen, W. Bras, Angew. Chem. Int. Ed. Ing. 34 (1995) 73.
[40] W.H. Dokter, T.P.M. Beelen, H.F. van Garderen, C.P.J. Rummens, R.A. van Santen, J.D.F. Ramsey, Colloids Surf. A 85 (1994) 89.
[41] S.L. Burkett, M.E. Davis, J. Phys. Chem. 98 (1994) 4647.
[42] H. Giesche, J. Eur. Ceram. Soc. 14 (1994) 189.
[43] P.P.E.A. de Moor, T.P.M. Beelen, R.A. van Santen, J. Phys. Chem. B 103 (1999) 1639.
[44] P.P.E.A. de Moor, T.P.M. Beelen, R.A. van Santen, L.W. Beck, M.E. Davis, J. Phys. Chem. B 104 (2000) 7600.
[45] G.D. Stucky, Q.S. Huo, A. Firouzi, B.F. Chmelka, S. Schacht, I.G. Voigt-Martin, F. Schüth, Stud. Surf. Sci. Catal. 105 (1997) 3.
[46] F. Schüth, Angew. Chem. Int. Ed. 42 (2003) 3604.
[47] W.C. Li, A.H. Lu, F. Schüth, Chem. Eur. J. 11 (2005) 1658.
[48] S.D. Kinrade, T.W. Swaddle, Inorg. Chem. 27 (1988) 4253.
[49] W.J. Roth, J.C. Vartuli, Stud. Surf. Sci. Catal. 157 (2005) 91.